Organic Process Research & Development **2008,** *12,* 646–654

Interpretation of Focused Beam Reflectance Measurement (FBRM) Data via Simulated Crystallization

Zai Qun Yu,*[,†] Pui Shan Chow,[†] and Reginald B. H. Tan[†,‡]

*Institute of Chemical and Engineering Sciences Limited, A*STAR (Agency for Science, Technology and Research), 1 Pesek Road, Jurong Island, Singapore 627833, and Department of Chemical and Biomolecular Engineering, National University of Singapore, 10 Kent Ridge Crescent, Singapore 119260*

Abstract:

Focused beam reflectance measurement (FBRM) has gained much popularity as a tool for particle system characterization both in crystallization research and in manufacturing. The precise interpretation of FBRM data, however, still remains an issue of some conjecture and dispute. This study examines the relationship among total counts of chord lengths, statistics of chord length distribution, particle number and average particle size in simulated crystallization, which involves selective introduction of predetermined particle populations into a suspension so as to simulate the occurrence of nucleation and crystal growth as detected by the FBRM. The number of particles and particle size distribution were known precisely. It was found that a linear correlation existed between the counts of chord lengths and the number of particles for monosized populations, but not in the case of a dynamic process where there was a significant change in particle size. Square-weighted mean chord lengths were found to be able to track changes in average particle size qualitatively in some cases. Measured chord length distributions of monosized particle populations differed significantly from theoretically constructed distributions. These results have important implications for the interpretation of practical FBRM data, including the necessity to review the principles used in the restoration of particle size distribution from measured chord length distributions.

1. Introduction

Particle number and particle size distribution (PSD) are two important state variables in crystallization processes. A reliable means of *in situ* tracking of both of them is highly desirable in academic research as well as commercial production for close monitoring and tight control of processes. Focused beam reflectance measurement (FBRM) has emerged as a promising process analytical technology (PAT) sensor for such a purpose.

In FBRM, a focused laser beam spinning at a high speed propagates into the slurry through a sapphire window mounted on the tip of a cylindrical probe. When the laser beam intersects the edge of a particle, some of it is backscattered to the detector installed in the same probe, and induces a rise signal in the circuit until it reaches the opposite edge of the particle. A chord length is thus registered. The product of risetime and tangential velocity of the spinning laser beam is a chord length. The measurement range of chord length depends on the scanning speed of the laser beam and is divided into a fixed number of linear channels in the hardware. Each count of chord length is recorded in a corresponding channel and a chord length distribution (CLD) is thus generated. Chord length counts grouped by channels are the primary data provided by FBRM. In addition, the control interface provides a variety of weighted or unweighted statistics of the primary data, e.g. total counts of chord lengths in all channels, mean chord length, median, standard deviation of CLD, etc., which are different statistical presentations of the primary data.

It is logical to expect a relationship between the total counts of chord length and the number of particles, and a linkage between CLD and PSD. Total counts of chord lengths have been found to change linearly and then nonlinearly with *solids concentration* as solids concentration vary from low to high.[1–3] However, the *number of particles* is different from solids concentration in that solids concentration can be broken down into two factors, i.e., the number of particles and particle size. This break down is necessary in order to describe a nucleating and growing system of particles. The relationship among total counts of chord length, *the number of particles* and particle size needs to be investigated. Based on the working principles of FBRM, a larger particle is more likely to be detected than a smaller one and therefore generates more counts. It is of utmost importance to decouple the effects of particle size and the number of particles on chord length counts if a correct relationship is to be constructed.

Intuitively, counts of chord length in different channels of FBRM statistics can be associated with the number of particles with different sizes. The counts of chord length in the range of $1-23\ \mu$m were chosen as an indication for fine particles by Kline et al. [4], while Scholl et al.[5] used the counts in the range of $1-10\ \mu$m to monitor nucleation. Still, the chord length counts in the range of $1-29\ \mu$m were associated with the number of particles of small size.[6] It seems that the choice of dividing points for fine and coarse chord length is somewhat random,

* Corresponding author. Telephone: +65 67963869. Fax: +65 63166183. E-mail: yu_zaiqun@ices.a-star.edu.sg.

† Institute of Chemical and Engineering Sciences Limited, A*STAR (Agency for Science, Technology and Research).

‡ National University of Singapore.

(1) Barrett, P.; Glennon, B. *Part. Part. Syst. Charact.* **1999**, *16*, 207–211.

(2) Heath, A. R.; Fawell, P. D.; Bahri, P. A.; Swift, J. D. *Part. Part. Syst. Charact.* **2002**, *19*, 84–95.

(3) Pearson, A. P.; Glennon, B.; Kieran, P. M. *J. Chem. Technol. Biotechnol.* **2004**, *79*, 1142–1147.

(4) Kline, B. J.; Saenz, J.; Stankovic, N.; Mitchell, M. B. *Org. Process Res. Dev.* **2006**, *10*, 203–211.

(5) Scholl, J.; Bonalumi, D.; Vicum, L.; Mazzotti, M.; Muller, M. *Cryst. Growth Des.* **2006**, *6*, 881–891.

(6) O'Sullivan, B.; Glennon, B. *Org. Process Res. Dev.* **2005**, *9*, 884–889.

Published on Web 06/19/2008

10.1021/op800063n CCC: $40.75

and subject to considerable arbitrary judgment. A more rational understanding of the link between counts of chord lengths and counts of particles in different size ranges is clearly needed.

Statistics of PSD by alternative sizing methods have been correlated linearly with those of CLD as reviewed comprehensively by Heath et al.[2] In general, researchers are divided in the selection of statistics and have come up with a variety of disparate equations, indicating the possible system-specific nature of these correlations. Moreover, a linear relationship prevails only in a certain size range even for the same system. The incongruence does not bode well for the quantitative analysis and interpretation of FBRM data. For example, does a stabilizing square-weighted mean chord length necessarily signify the termination of crystal growth? Which statistics of CLD reflect the dynamics of crystallization most closely and faithfully, if at all?

First-principles reconstruction of complete PSD from CLD has been attempted for quite some time, applied to spherical and ellipsoidal [2,7,8] shapes in earlier years to more general shapes lately.[9–13] This approach, or its variations, has been used in a few kinetics studies.[14,15] The collection of FBRM data can be imagined as a two-step process: (a) the projection of particle silhouette on a surface parallel to the probe window (a particle may take random orientations with respect to the probe window which leads to different silhouettes); (b) the metering of chord lengths on the projection (the alignment of the particle center with the laser beam is also random which leads to different chord lengths). *If the backscattering of light is ideal,* the CLD of a single particle can be calculated. Then the CLD of a particle population is given by superposition of single-particle CLDs. Conversely, PSD can be restored from CLD by solving an inverse problem. Ideal backscattering means the focused laser beam has no width, and the reflection and detection of light are not affected by the distance between particles and focal point, the refractive indices of suspension medium and the particle, or overcrowding of particles in dense slurries. Although researchers can verify their restoration by comparing with alternative sizing methods, the assumptions adopted therein remain a practical hurdle for the wider application of first-principles reconstruction in real systems.

The interesting and relevant experimental work by Ruf et al.[16] has seriously challenged the assumptions in theoretical reconstruction of PSD. In their studies, a ceramic sphere was fixed in front of the FBRM probe window which falls on the sweeping path of the laser beam. FBRM data were collected with different distances between the spherical particle and probe window, different alignments of the laser beam with the spherical axis, and different working media. One significant conclusion of their work was that the actual CLD of the ceramic sphere depended heavily on its distance to the focal point of the laser beam, and it deviated significantly from its theoretical value as the sphere went away from the focal point "due to the weakening and broadening of the laser beam that makes it more difficult for the FBRM signal processing to detect precisely the boundary of the particle". This fact has hitherto been neglected in all studies of first-principles reconstruction. In addition, surface properties and relative refractive indices were also found to be very influential in CLD measurements, which have not been accounted for in these studies either.

At this juncture, a number of uncertainties have been raised about the practical interpretation of FBRM data. This contribution attempts to shed some light on these uncertainties, and is arranged as follows. Theoretical mapping from PSD to CLD, as used in first principles restoration approaches reported in previous studies, will be presented in the next section. A series of monosized standard polystyrene spheres with different sizes are added in the crystallizer in such a sequence, quantity, and proportion that from the perspective of the FBRM, crystallizations with various dynamics are taking place (hence the term simulated crystallization). The FBRM responses are then analyzed and examined in light of the actual particle populations which have been known *a priori*. The calculated CLD from theoretical mapping will be compared with measured CLD of these standard spheres. The use of spherical particles in experiments eliminates the shape effects on CLD and simplifies data analysis. In addition, suspensions of glycine crystals, "real" systems as opposed to the "ideal" system of polystyrene spheres, will be also used in the experiment to corroborate the conclusions.

2. Theoretical Mapping of PSD to CLD

2.1. CLD of Single Spheres. In FBRM hardware, the chord length range of 0.25−1024 μm is divided into 1324 linear channels. There are 400 channels in the range of 0.25−100 μm, and the width of each channel is 0.25 μm. In the range of 100−1024 μm, each channel spans a width of 1 μm. The 1324 channels can be regrouped according to the user's preference, into 100 channels for example. In this study, the calculation of single-sphere CLD is performed in line with the hardware configuration of FBRM machine, i.e., in 1324 channels, with the purpose of comparability between theoretical and measured CLD. The channels are then regrouped into intervals of 2 μm for both theoretical and measured CLD. The theoretical and experimental normalized CLDs (unweighted) will be presented with a linear progression of x-axis and they have the same shape with their corresponding chord length counts density distributions. Logarithmic progression of x-axis is preferred sometimes in practice for it produces a better-looking shape of CLD than linear progression by uneven grouping of chord lengths. As the application of weighting to CLD calculation, it does nothing to improve signal/noise ratio but represents original data in a different way.

Referring to Figure 1 a, the probability $p_i(d_j)$ of the laser beam of FBRM scanning between chord length L_i and L_{i+1} of a single sphere with a diameter of d_j can be expressed as:[8,10]

(7) Tadayyon, A.; Rohani, S. *Part. Part. Syst. Charact.* **1998**, *15*, 127–135.
(8) Hukkanen, E. J.; Braatz, R. D. *Sens. Actuators, B* **2003**, *96*, 451–459.
(9) Worlitschek, J.; Hocker, T.; Mazzotti, M. *Part. Part. Syst. Charact.* **2005**, *22*, 81–98.
(10) Li, M.; Wilkinson, D. *Chem. Eng. Sci.* **2005**, *60*, 3251–3265.
(11) Li, M.; Wilkinson, D.; Patchigolla, K. *Chem. Eng. Sci.* **2005**, *60*, 4992–5003.
(12) Pons, M.-N.; Milferstedt, K.; Morgenroth, E. *Chem. Eng. Sci.* **2006**, *61*, 3962–3973.
(13) Nere, N. K.; Ramkrishna, D.; Parker, B. E.; Bell, W. V.; Mohan, P. *Ind. Eng. Chem. Res.* **2007**, *46*, 3041–3047.
(14) Worlitschek, J.; Mazzotti, M. *Cryst. Growth Des.* **2004**, *4*, 891–903.
(15) Togkalidou, T.; Tung, H. H.; Sun, Y.; Andrews, A. T.; Braatz, R. D. *Ind. Eng. Chem. Res.* **2004**, *43*, 6168–6181.
(16) Ruf, A.; Worlitschek, J.; Mazzotti, M. *Part. Part. Syst. Charact.* **2000**, *17*, 167–179.

$$p_i(d_j) = \begin{cases} \sqrt{1-\left(\frac{L_i}{d_j}\right)^2} - \sqrt{1-\left(\frac{L_{i+1}}{d_j}\right)^2}, & \text{for } L_i < L_{i+1} \le d_j \\ \sqrt{1-\left(\frac{L_i}{d_j}\right)^2}, & \text{for } L_i \le d_j \le L_{i+1} \\ 0, & \text{for } d_j < L_i < L_{i+1} \end{cases} \quad (1)$$

When d_j is fixed, $[p_1(d_j), p_2(d_j)...p_R(d_j)]$ is taken to be the normalized CLD of a single sphere with R being the number of chord length channels and $\sum_i p_i(d_j) = 1$. The CLD of a sphere with a diameter of 100 μm can be calculated from eq 1 and is shown in Figure 1 b with a channel width of 2 μm. When both i and j vary, $p_i(d_j)$ is an $R \times S$ matrix, written in a compact form as **P** (mapping matrix). S is the number of discrete diameters.

2.2. CLD of a Population of Spheres. The discretized size distribution of a population of spheres can be written as a vector $\mathbf{N} = [n(d_1),n(d_2)...n(d_S)]^T$, where $n(d_j)$ represents the number of particles at a discrete diameter d_j. In this study, d_j takes the values of 1 μm, 2 μm,..., which are found to be sufficiently fine for computational purposes. The normalized size distribution is then denoted as **X** with entries being:

$$x(d_j) = \frac{n(d_j)}{\sum_j n(d_j)} \quad (2)$$

The normalized CLD of a particle population is represented as $\mathbf{C} = [c_1,c_2,...,c_R]$ with $\sum_i c_i = 1$, and the subscripts signify different channels. **C** can be computed by superposition of the CLDs of all the constituent particles.

Two different methods have been adopted to calculate the CLD of a population of spheres. The following formulas were adopted by Hukkanen and Braatz[8] and Li and Wilkinson:[10]

$$\mathbf{C} = \mathbf{P}^T \times \mathbf{X} \quad (3)$$

In another method, diameter-weighted size distribution was used:[9]

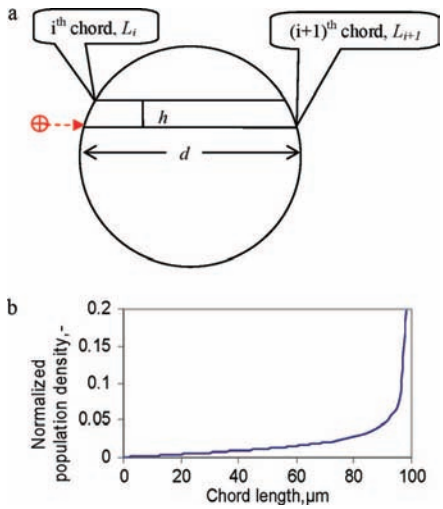

Figure 1. **(a) Two chord lengths of a sphere (b) the theoretical CLD of a 100 μm sphere.**

$$y(d_j) = \frac{n(d_j)d_j}{\sum_j n(d_j)d_j} \quad (4)$$

The diameter-weighted size distribution is denoted as $\mathbf{Y} = [y(d_1),y(d_2),...y(d_R)]^T$. The CLD of a particle population is then computed as:

$$\mathbf{C} = \mathbf{P}^T \times \mathbf{Y} \quad (5)$$

The application of diameter weighting may be motivated by the hypothesis that larger particles are more likely to be detected by the laser beam. For a population of spheres with a narrow PSD, eqs 3 and 5 make little difference. Only equation 5 is employed in this study. However, eqs 3 and 5 may lead to significantly different CLD for a general PSD.

3. Experimental Section

3.1. Standard Polystyrene Spheres. Microparticles based on polystyrene were obtained from Sigma-Aldrich, with their specifications listed in Table 1. Microscopic photos of three specifications are shown in Figure 2.

Microparticles of different sizes are marketed in suspension form with a solid concentration of 10 wt % (100 mg polystyrene particles/mL suspension). Samples were drawn with a specified number of particles according to the equation below:

$$M = n\rho\frac{1}{6}d^3 = 0.1\,V \quad (6)$$

where M and d stand for the mass and diameter of particles. n is the number of particles and V is volume of suspension. Then the relative number of particles of different sizes can be controlled according to the following equation:

$$\left(\frac{d_1}{d_2}\right)^3 = \frac{V_1}{V_2} \quad (7)$$

where subscripts 1 and 2 denote particle sample 1 and particle sample 2, respectively. Deionized water was used to dilute original suspensions.

3.2. Glycine Crystals. Crystals of glycine (Aldrich-Sigma, 99%) were classified by sieves, and the nine size ranges include 106−125, 125−150, 150−180, 180−212, 212−250, 250−300, 300−355, 355−425, and 425−500 μm. The photos of crystal samples are given in Figure 3. Ethanol was used to prepare suspensions of different slurry density to avoid the possible effects of Ostwald ripening in water. There was no visible crystal breakage after measurement.

Table 1. **Specifications of microparticles**

catalogue no.	average size, μm	standard deviation, μm
72986	10	0.2
74491	20	0.3
84135	30	0.4
90768	150	4.5
16435	200	4.0
19429	250	6.5

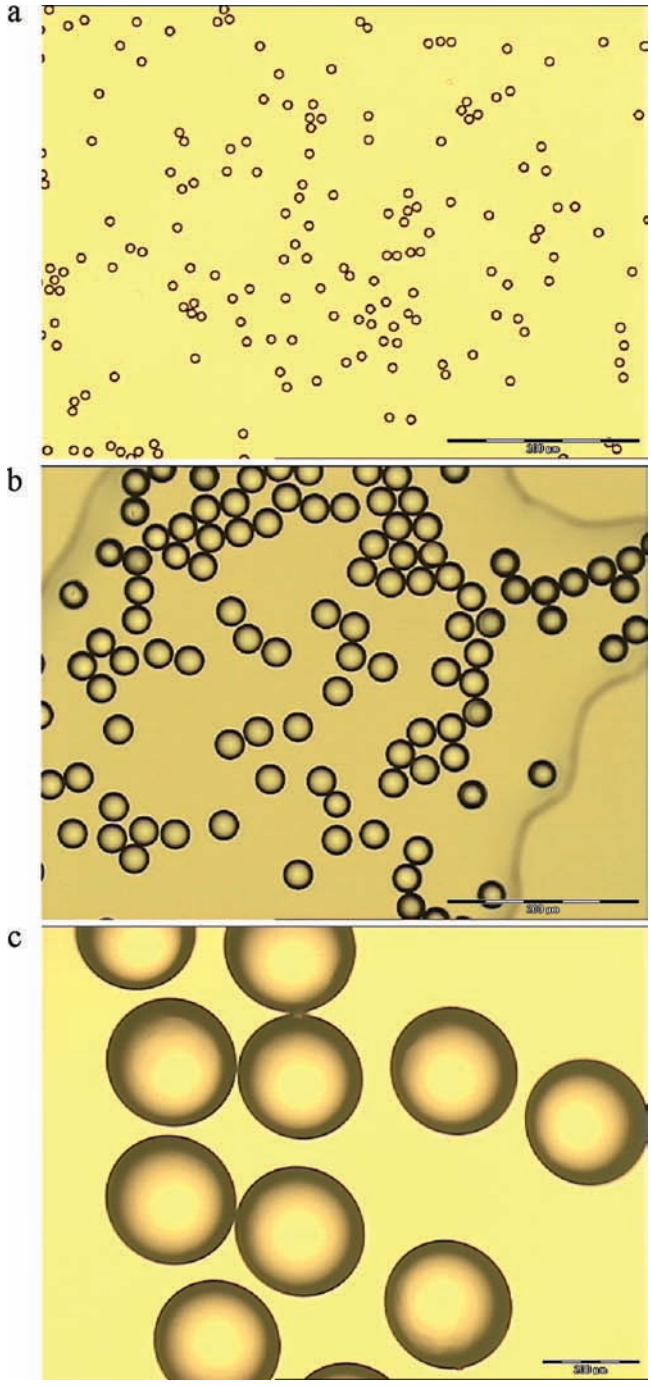

Figure 2. **Photos of standard particles based on polystyrene (a) 10 μm, (b) 30 μm, (c) 250 μm. Scale bars represent 200 μm.**

3.3. Experimental Setup. Experiments were carried out on the probe support stand provided by Lasentec company, equipped with a 100 mL beaker, an electric motor-driven stirrer and a FBRM probe (model S400). The FBRM probe tip was inclined towards the flow direction of suspension and located near the beaker wall. The suspension volume in the beaker was kept at 80 mL, and the rotation speed of stirrer was maintained at 400 rpm for all experiments to suspend particles of all sizes sufficiently while avoiding the entrapment of air bubbles. The volume of suspension was not of significance for this study as compared to slurry density which was well defined throughout.

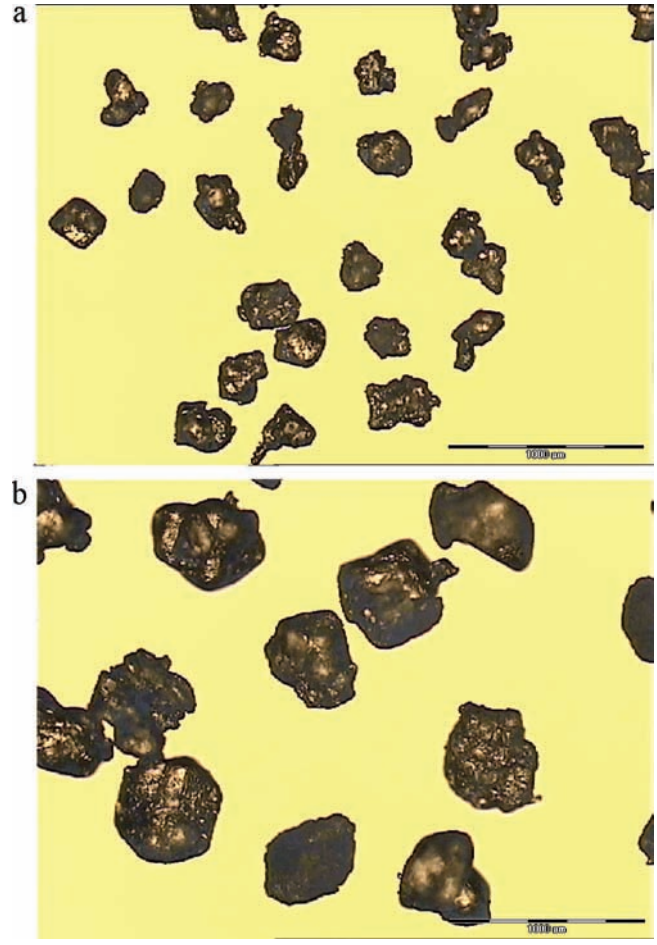

Figure 3. **Photos of classified glycine crystals (a) 180−212 μm, (b) 355−425 μm.**

The instrument used in this study can be switched between fine and coarse discrimination electronics (abbreviated as F and C electronics hereafter). F and C electronics are two low-pass filter options differing in the cutoff frequencies [17] and there is no definite yardstick as to which one to use in any particular circumstance. With respect to studies involving quantitative interpretation of FBRM data, it is necessary to adhere to only one of the two modes. F electronics was selected for most experimental runs, with a measurement duration of 10 s. Readings from some suspensions with coarse electronics were also recorded to compare the relative ability of F/C electronics to track changes in particulate dynamics. The CLDs and statistics shown in this contribution were statistically reliable in that they did not change anymore with further increasing of slurry density.

4. Results and Discussion

Three scenarios of crystallization were simulated using polystyrene particles in the first three subsections, i.e., pure nucleation, pure crystal growth, and nucleation with simultaneous crystal growth. In the fourth subsection, measurement results with glycine crystals were presented and discussed.

4.1. Pure Nucleation. During nucleation, the number of crystals increases, while the size distribution remains narrow and almost unchanged. Microparticles of the same specification were added to the beaker in increments to simulate nucleation

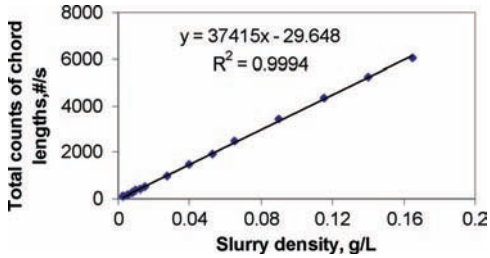

Figure 4. **Relationship between total counts of chord lengths and the slurry density.**

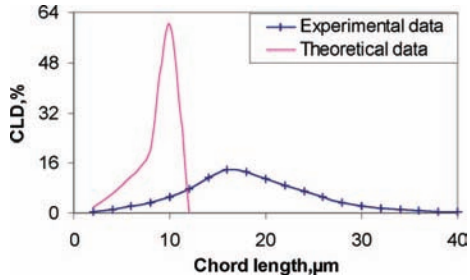

Figure 5. **Comparison of measured and theoretical CLDs of a sphere population.**

events. The changes in the five most common statistics of CLD were examined, i.e., total counts of chord lengths, unweighted mean chord length, unweighted median, unweighted mode and square-weighted (sq-wt) mean chord length.

Microparticles of 1 μm were used at first and it was found that they could not be detected by FBRM even after the suspension had become opaque at relatively high solid concentration. Therefore, the next higher size (10 μm) was used to simulate nucleation.

The FBRM total counts of chord lengths are plotted against slurry density in Figure 4 which shows an excellent linear correlation. It can be seen that for monosized particles the counts of chord lengths can be used reliably to represent the number of particles in a certain range. However, it is to be stressed that this result is strictly valid only for a population of homogeneously sized spheres. Nevertheless, the result would be valuable in measuring the number of particles and nucleation rate in the early stages of spontaneous primary nucleation.

A particle vision measurement (PVM) probe was inserted into the slurry after FBRM measurement to observe particles visually; it was found that there was no aggregation of particles, which confirmed it was single particles, instead of aggregates, that were being measured. The excellent linear correlation between total counts of chord lengths and the number of particles also corroborates the absence of aggregation, as a dynamic aggregation process would show an increasing deviation from linearity.

Other statistics used to approximate particle size yielded different values. Unweighted mean, unweighted mode, and unweighted median of chord lengths were 17.2, 15.0, and 16.8 μm, respectively, while sq-wt mean chord length was 24.5 μm. All these statistics are relatively far from the true value of 10 μm.

The measured CLD and theoretical prediction as described in section 2 are compared in Figure 5. Theoretical CLD dropped to zero abruptly beyond 10 μm, as expected from Figure 1, while measured CLD spanned a much wider range up to 40

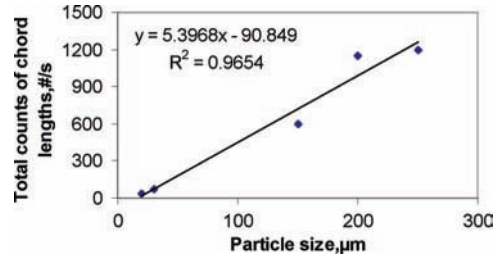

Figure 6. **Changes in total counts of chord lengths with particle size. Slurry density changed from 0.00250 g/L with particles of 20 μm to 4.88 g/L with particles of 250 μm.**

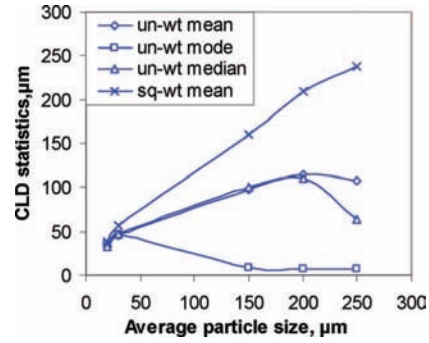

Figure 7. **Relationship between various statistics of CLD and particle size.**

μm. Overestimation of particle size in the case of small particles was also reported by Ruf et al.[16] They attributed it to the conical shape of the laser beam. The diameter of the laser beam swells as it propagates away from the probe window, which makes particles look larger than their true sizes. The obvious discrepancy presents a greater practical difficulty when trying to effect a first principles restoration of PSD from measured CLD.

4.2. Pure Crystal Growth. In this series of experiments, the same number of microparticles of 20, 30, 150, 200, 250 μm were put in the beaker separately. The particles were removed after each measurement, and replaced with the next higher size. When perceived in the ascending order of particle sizes, this simulates ideal crystal growth, with each crystal growing at the same rate. The number of particles of different sizes was calculated according to eq 7.

The total counts of chord lengths changed with particle size as the number of particles was kept constant for all size specifications as demonstrated in Figure 6, meaning it is not advisable to approximate the number of particles by the counts of chord lengths in a dynamic process where there is significant change in particle size. The trend reveals that larger particles have more chances to be detected by FBRM, and the relationship between them is approximately linear, which justifies the length-weighting as used in eq 5.

The evolution of the FBRM statistics unweighted mean, unweighted mode, unweighted median, and sq-wt mean of the CLD during the progress of simulated ideal crystal growth is shown in Figure 7.

Figure 7 reveals some surprising results. First, the unweighted mode decreased to a very low value (below 10 μm) for particle sizes beyond 150 μm. Second, the unweighted mean and median of the CLD increased with increasing particle size and then decreased beyond 200 μm. Third, the values of unweighted mode, median, and mean were well below the true

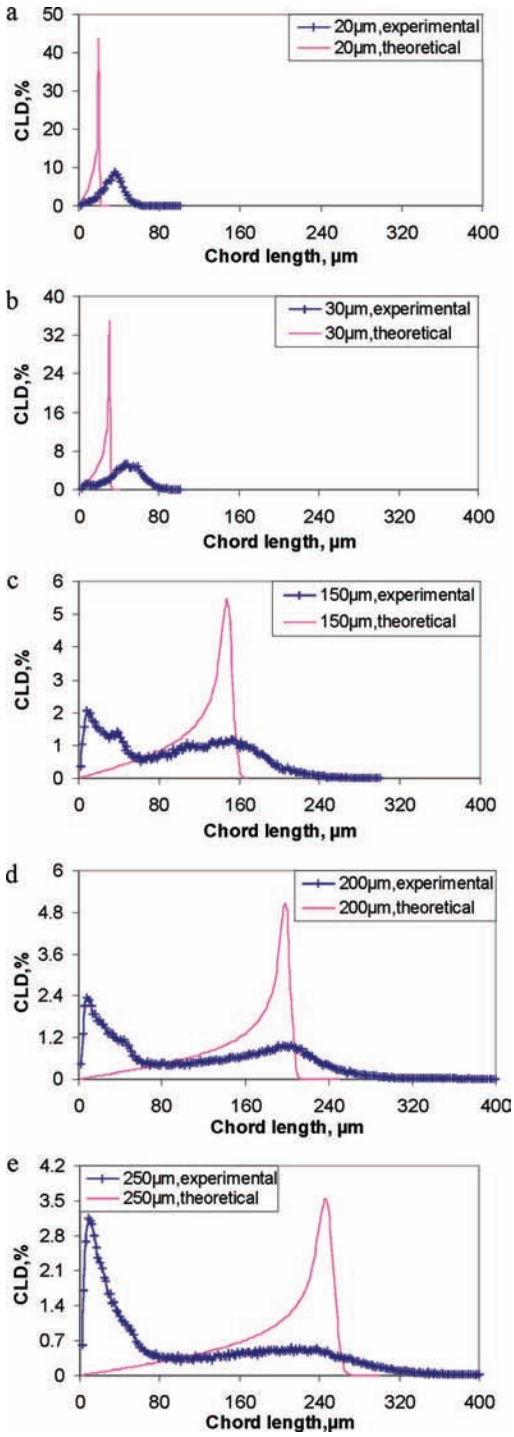

Figure 8. **Comparison of measured and theoretical CLDs of sphere populations with different sizes, (a) 20 μm, (b) 30 μm, (c) 150 μm,(d) 200 μm,(e) 250 μm.**

particle size. Somewhat surprisingly, the sq-wt mean of CLD followed the true particle size rather closely, which appears to be completely fortuitous.

In order to understand these trends better, it is necessary to study the full CLD measured at each stage, and these are presented in Figure 8. Theoretical CLDs are also illustrated for comparison.

It can be seen that theoretical CLD maintained its characteristic shape as the position of a single peak shifted towards right with increasing particle sizes. In contrast, an anomalous second peak of "small" chord lengths evolved gradually in small chord length as particle size increased, which causes the surprising results. Recall that the measurements were carried out with pure samples of monosized spherical particles and the anomalous peaks cannot be attributed to the existence of "fines". On the contrary, the occurrence of the anomalous second peak and its increasing proportion seems to be inherent to FBRM. Ruf et al.[16] demonstrated that particles are "visible" to FBRM only within a rather well-defined region whose depth extends with increasing particle size. "Visible" means FBRM can detect the presence of particles, not necessarily the true boundaries of particles. They found that when particles move from the probe window towards the far end of this region, the proportion of small chord lengths in total counts increases rather dramatically. The farther part of this region can be deemed as the source of noises. In the case of larger particles, the stretched region also implies an enhanced source of noises which results in the increasing proportion of the second peak. Another explanation for the occurrence of disproportionate small chord lengths is random "chord splitting".[17] The backscattered light may vary greatly in intensity due to various reasons such as surface roughness, and the filtered signal by F electronics could fall below the threshold before the laser beam reaches the opposite edge of the intersected particle. As a result, more than one chord length is recorded in one intersection of laser beam with the particle, yielding excessive counts of short chord lengths. C electronics can reduce chord splitting to some degree. However, it has its own demerits; for example, it may fail to resolve individual particles in dense suspensions.

The ever-increasing proportion of short chord lengths obtained from a crystal growth process brings about insurmountable difficulty in correlating the number of particles with counts of chord lengths in a certain range. Contradictory to the assumed linkage between counts of chord lengths in different channels and the number of particles with corresponding sizes, an increase in short chord lengths does not necessarily mean the occurrence of nucleation.

4.3. Simultaneous Nucleation and Crystal Growth. Microparticles of different sizes were put in the beaker consecutively in the ascending order of their sizes without replacement (different from the previous scenario). Particles of various sizes accumulated in the slurry during the process, which could be deemed as a crystallization process with simultaneous nucleation and crystal growth.

The number of particles and average particle size were increasing simultaneously, which were reflected by sq-wt mean chord length in Figure 9. Attempts have not been made to correlate sq-wt mean chord length with average particle size. However, sq-wt mean chord length really followed the volume-based average particle size closely. Again, it should be mentioned that the relationship between them is system dependent and may be valid only for the model system used in this study

(17) Kail, N.; Briesen, H.; Marquardt, W. *Part. Part. Syst. Charact.* **2007**, *24*, 184–192.

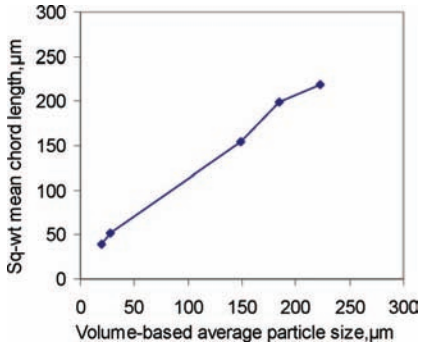

Figure 9. **Relationship between sq-wt mean chord length and volume-based average particle size.**

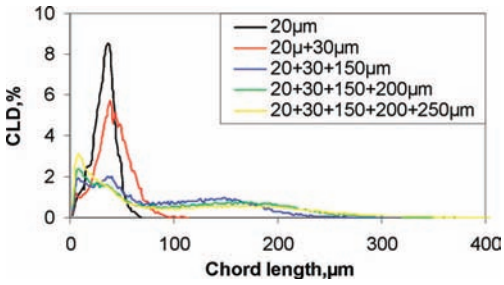

Figure 10. **Changes in normalized CLDs with the addition of particles of different sizes.**

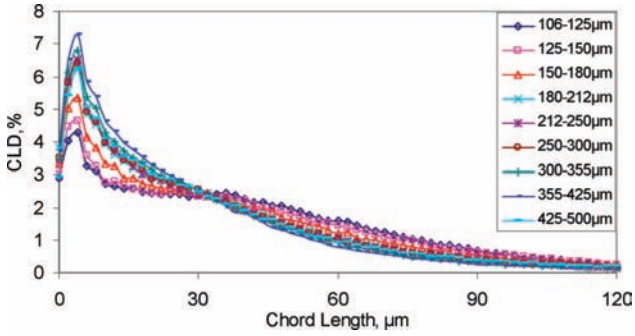

Figure 11. **CLDs of glycine crystals of different size ranges.**

Figure 10 shows the normalized CLDs when nucleation and crystal growth are taking place. Before the particles of 150 μm were put into the suspension, there was only one peak in the CLDs. After that, another peak developed in large chord length, indicating changes were occurring in the system.

4.4. Simulated Crystal Growth of Glycine. As shown in Figure 8 a−e, the measured CLDs of monosized polystyrene spheres changed in shape with increasing particle size, and the proportion in small chord length increased, which prompts us to check if this anomaly of CLDs is specific to polystyrene particles. Sieved glycine crystals of different size ranges and proportionate amounts of ethanol were put into the beaker to prepare suspensions. FBRM data collected in the series of suspensions, when observed in the ascending order of size range, simulated the process of crystal growth. The number of crystals was not controlled as we were concerned only with CLD instead of counts of chord lengths. The CLDs collected from different suspensions are shown in Figure 11.

From Figure 11 it can be seen that the CLDs of glycine crystals have a shape similar to those of relatively large polystyrene spheres, exhibiting a peak at small chord lengths. We conclude that the obvious difference between theoretical

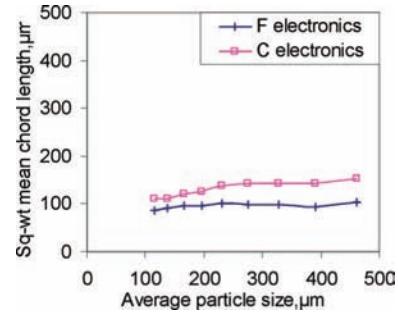

Figure 12. **Square-weighted mean chord length vs particle size (average sieve aperture).**

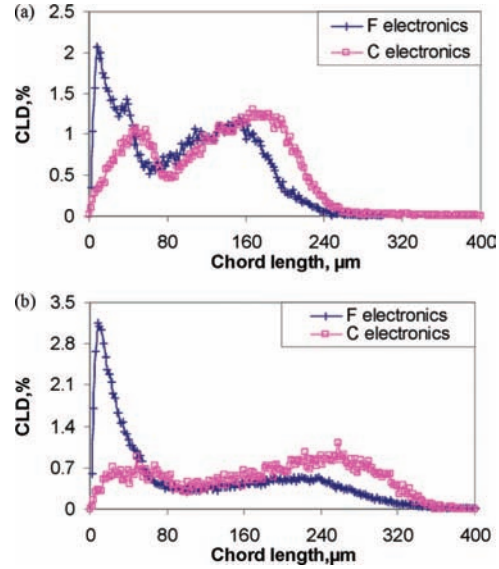

Figure 13. **Comparison of CLDs with F and C electronics (a) microparticles of 150 μm (b) microparticles of 250 μm.**

and measured CLD of polystyrene spheres is not an isolated case and the anomaly at small chord lengths is inherent in measurements with F electronics.

The statistic of sq-wt mean chord length seems to lose its ability to follow changes in particle size after particle size exceeds 250 μm in the case of glycine crystals, as shown by the curve labeled as F electronics in Figure 12. In general, our results indicate that the interpretation of FBRM data is difficult to generalize. Interpretation of FBRM data from large-scale crystallizers must be preceded by careful observations of the same system in the laboratory. It is not advisable to simply relate the number of chord lengths and various statistics with particle counts and particle size.

4.5. Comparison of Readings with Fine and Coarse Discrimination Electronics. The main results shown hitherto have been collected with F electronics. Different CLDs will be obtained from the same suspensions if C electronics is selected. It is worthwhile to look into the features of CLDs with C electronics and its ability to follow size change.

Figures 13 and 14 show the normalized CLDs of polystyrene microparticles and glycine crystals, respectively, with F and C electronics. It can be seen that the peaks at small chord lengths are greatly reduced with C electronics, agreeing with the results by Kail et al.[17] The resulting CLDs of polystyrene particles still differ obviously from theoretical ones illustrated in Figure 8, and it

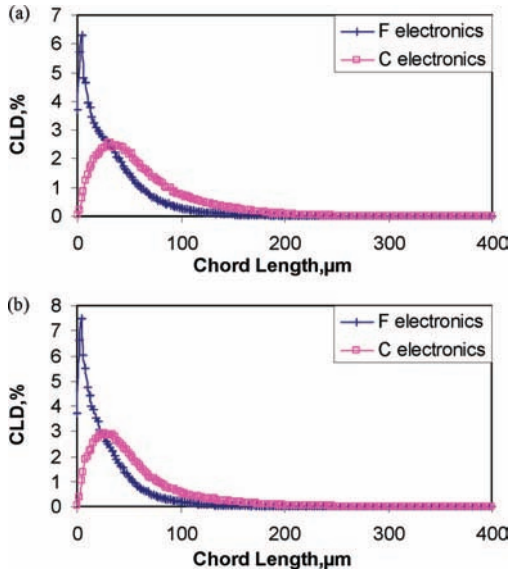

Figure 14. **Comparison of CLDs with F and C electronics (a) glycine crystals of 180−212 μm (b) glycine crystals of 355−425 μm.**

can be deduced that chord-splitting is not the only reason for such a discrepancy. It was also found that F electronics registered more total counts of chord lengths than C electronics, which means more counts of short chord lengths were dropped than those of long chord lengths by C electronics. Consequently, sq-wt mean chord length became larger in C electronics. Nevertheless, the ability to track changes in particle size of glycine crystals did not improve with C electronics, as shown in Figure 12.

4.6. Application of FBRM. FBRM is based on different working principles from alternative sizing techniques. The failure of universal correlation with alternative sizing methods and difficulty in restoring PSD from CLD do not detract from the usefulness of FBRM in that it responds well to particulate dynamics as has been shown in recent studies.[18–24] For example, Chew et al.[25] developed a novel FBRM technique to control internal seed generation and batch-to-batch consistency of crystal product PSD. In the three scenarios investigated in this study, changes in the number and PSD of crystals were reflected by total counts of chord lengths and CLD. The problem arises in attempting to interpret FBRM data quantitatively.

Construction of soft sensors using FBRM data for process performance or quality of particles seems to be a good method. For example, Togkalidou et al. [26] correlated the chord length counts in 10 channels with the logarithm of filtration resistance of pharmaceutical crystals by using chemometrics. Negro et al. [27] established a soft sensor for the properties of asbestos cement by analyzing in-process FBRM data using artificial neural networks. The use of other online PAT sensors at the same time will afford necessary complementing information to effect more reliable monitoring of particulate processes.

5. Conclusion

Spherical particles of polystyrene were used to investigate the relationship between the number of particles, PSD, counts of chord lengths, and CLD. The simplicity of particle shape enabled us to concentrate on the basic aspect of particle sizing. It was demonstrated through rigorous experiments that total counts of chord lengths are influenced by both the number of particles and particle size, in agreement with the findings of Pearson et al.[3] They could be correlated linearly with the number of particles for monosized populations. At the same time, it is not advisable to approximate the number of particles in a dynamic process using counts of chord lengths if there is a significant change in particle size. Square-weighted mean chord length was found to be able to track changes in particle size qualitatively for spherical polystyrene particle suspensions, but was unsuccessful for glycine crystal suspensions. The results from this study purport that care must be exercised in generalizing empirical correlations between CLD with PSD.

Theoretical chord length distribution of particle populations were also constructed according to the procedures reported in the literature. Measured chord length distributions of monosized particle populations with both F and C electronics were found to differ significantly from theoretical values, which suggests strongly that any attempt at first principles recovery of PSD from measured CLD data based on ideal backscattering of light should be approached with great care.

Experiments with polystyrene particles and glycine crystals showed that C electronics dramatically subdued the peak at small chord lengths, possibly by reducing the occurrence of chord splitting. However, the ability of sq-wt mean chord length to track size change did not improve as compared with F electronics.

Future work on the use and interpretation of FBRM data remains to be strengthened along two possible lines. The first is to treat the backscattering process as a black box and focus on the correlation of FBRM data with PSD or process performance of suspensions through rigorous data mining. The second is to delve into the backscattering process and address the discrepancy between measured CLD and predicted CLD by current models. The first approach is more easily implemented but is difficult to extrapolate to other systems or even other size ranges of the same system used for correlation. The second is more challenging because the physics of backscattering has yet to be understood comprehensively.

(18) Black, S. N.; Quigley, K.; Parker, A. *Org. Process Res. Dev.* **2006**, *10*, 241–244.
(19) Scott, C.; Black, S. *Org. Process Res. Dev.* **2005**, *9*, 890–893.
(20) Yu, Z. Q.; Chow, P. S.; Tan, R. B. H. *Ind. Eng. Chem. Res.* **2006**, *45*, 438–444.
(21) Yu, Z. Q.; Tan, R. B. H.; Chow, P. S. *J. Cryst. Growth* **2005**, *279*, 477–488.
(22) Birch, M.; Fussell, S. J.; Higginson, P. D.; McDowall, N.; Marziano, I. *Org. Process Res. Dev.* **2005**, *9*, 360–364.
(23) Al Nasser, W. N.; Shaikh, A.; Morriss, C.; Hounslow, M. J.; Salman, A. D. *Chem. Eng. Sci.* **2008**, *63*, 1381–1389.
(24) Hu, X. H.; Cunningham, J. C.; Winstead, D. *Int. J. Pharm.* **2008**, *347*, 54–61.
(25) Chew, J. W.; Chow, P. S.; Tan, R. B. H. *Cryst. Growth Des.* **2007**, *7*, 1416–1422.
(26) Togkalidou, T.; Braatz, R. D.; Johnson, B. K.; Davidson, O.; Andrews, A. *AIChE J.* **2001**, *47*, 160–168.
(27) Negro, C.; Alonso, A.; Blanco, A.; Tijero, J. *Ind. Eng. Chem. Res.* **2006**, *45*, 197–205.

Acknowledgment

This work was supported by the Science and Engineering Research Council of A*STAR (Agency for Science, Technology and Research), Singapore.

Nomenclature

d	diameter of particles, μm
d_j	diameter of particles at discrete point j, μm
L_i	chord length at discrete point I, μm
n	number of particles, -
$p_i(d_j)$	the probability of the laser beam scanning between chord length L_i and L_{i+1} of a single sphere with a diameter of d_j, -
M	mass of particles, g
R	the number of chord length channels, -
S	the number of discrete diameters, -
V	volume of suspension, μm^3
ρ	density of particles, g/μm^3
C	normalized CLD of a particle population, vector
P	mapping matrix
N	number-based particle size distribution, vector
X	normalized number-based particle size distribution, vector
Y	length-weighted size distribution, vector

Abbreviations

FBRM	focused beam reflectance measurement
CLD	chord length distribution
PAT	process analytical technology
PSD	particle size distribution
PVM	particle vision measureme

Received for review March 20, 2008.

OP800063N